Stereo Rectification for X-ray Data Consistency Conditions

André Aichert, Jérôme Lesaint, Tobias Würfl, Rolf Clackdoyle, Laurent Desbat and Andreas K. Maier

***Abstract*—Data consistency conditions (DCC) allow for the compensation of measurement errors and geometric inaccuracies of X-ray computed tomography (CT). Epipolar Consistency (EC), in particular, states that any two X-ray projections contain redundant information on epipolar lines. Recently, a fan-beam DCC was applied to cone-beam projections by re-projection and weighted integration in a virtual detector. It is related to EC, since the redundant fans lie in a common epipolar plane. This paper observes that the re-projection to a common virtual detector is merely an instance of stereo rectfication known from computer vision and shows how rectifying homographies can be used to generally express these DCCs. We derive an algorithm which allows for the evaluation directly in the original detector planes, without the need for memory- and time-intensive warping of all image pairs. Since the presented algorithm does not require a derivative, it may prove beneficial in applications, which aim at the estimation of absolute intensities, rather than geometry or motion. We have validated the equations in this paper numerically with phantom data.**

I. Introduction

Epipolar Consistency (EC) is a type of data consistency condition in X-ray computed tomography, which exploits redundancies along epipolar lines in two X-ray projection images [1]. They have been used for the correction of various artifacts in computed tomography. EC states that the orthogonal derivative of integrals over two corresponding epipolar lines are identical. An alternative formulation has been presented, which uses the ramp-filter instead of a derivative [3]. Recently, a similar set of conditions has been applied to calibration correction in rotational CT [4]. The authors show that by means of a reprojection to a virtual detector plane, pair-wise fan-beam consistency conditions (FBCC) can be applied [5]. The main difference between these conditions is (1) integration along epipolar lines followed the derivative or ramp filter orthogonal to epipolar lines versus (2) an integral along epipolar lines weighted by the distance of each pixel to the baseline. The derivative emphasizes high-frequency information, which improves alignment of edges in motion correction application. However, artifact correction methods which correct for intensity changes (e.g. beam-hardening, scatter or extinction) may benefit from the absolute intensity information still available through the latter FBCC. A major drawback of the algorithm is that re-projection to a common virtual detector is different for any two projections. Consequently, n projection images would produce $n \cdot (n-1)$ pairs of rectified 2D images.

André Aichert, Tobias Würfl and Andreas K. Maier are with the Pattern Recognition Lab, Friedrich-Alexander Universität Erlangen-Nürnberg, Germany.

Jérôme Lesaint, Rolf Clackdoyle and Laurent Desbat are with the TIMC-IMAG laboratory, CNRS UMR 5525 and Université Grenoble Alpes, Grenoble, France

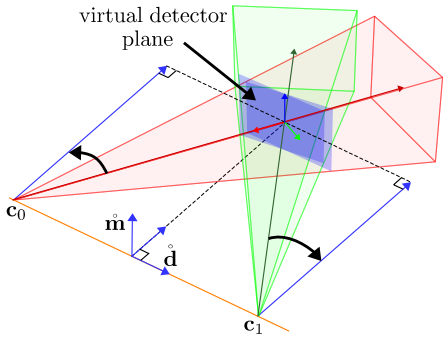

Figure 1. The stereo baseline connecting $\mathbf{c}_0$ and $\mathbf{c}_1$ and its relation to the virtual detector plane.

This paper observes that re-projection of two central projections to a common plane is an instance of the stereo rectification problem in computer vision [2]. Stereo rectification is the process by which two rectifying homographies are applied to a pair of images to produce identical corresponding epipolar lines which are parallel to the horizontal image axis. It is the well-understood first step for the computation of a depth-map from two visible light images.

By application of standard computer vision techniques, Section II extends the FBCC algorithm by Lesaint et al. [4] to general projection matrices and thus non-circular trajectories. In Section III we show how to evaluate the presented DCCs without explicit projection of all pairs of images. This drastically reduces the computational cost and amount of memory required, thus rendering practical application feasible. We validated this work on real data of a pumpkin phantom.

II. Rectification by Projection onto a Plane

A. Rectification

Consider two X-ray source-detector geometries defined by the projection matrices $\mathbf{P}_0$, $\mathbf{P}_1 \in \mathbb{R}^{3\times4}$. This section discusses how to find two rectifying homographies $\mathbf{H}_0$, $\mathbf{H}_1 \in \mathbb{R}^{3\times3}$, which transform projection images such that the respective image planes of $\mathbf{H}_0\mathbf{P}_0$ and $\mathbf{H}_1\mathbf{P}_1$ are parallel to the baseline, while corresponding epipolar lines are equal and parallel to the u-axis. We will do this by re-projecting the image data to a common virtual detector plane. The source positions in

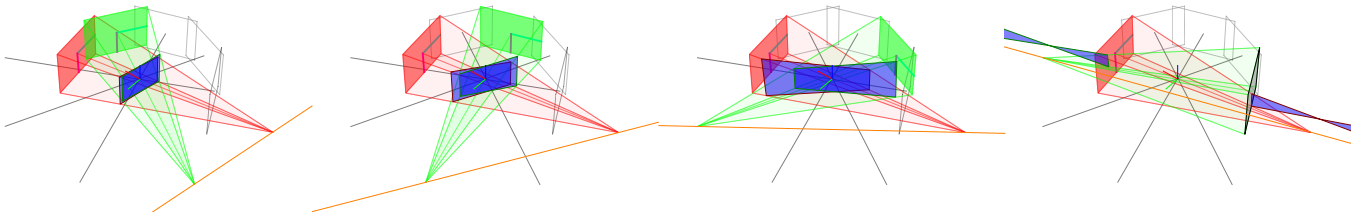

Figure 2. Rectified projection data is subject to increasingly strong distortion as the primary angle difference between the two projections increases. Example of a typical circular CT trajectory of a Siemens Artis Zeego: (1) little distortion up to $\approx 45°$, (2) considerable distortion at $\approx 90°$, (3) method is beginning to break down after $\approx 135°$, and (4) rectification not sensible for opposing views.

homogeneous coordinates $\mathbf{c}_0 \cong (C_0^0, C_0^1, C_0^2, 1)^\top \in \text{null}(\mathbf{P}_0)$ and $\mathbf{c}_1$, accordingly, define the stereo baseline, where $\cong$ denotes equality up to scale, define the stereo baseline. Its direction $\mathring{\mathbf{d}} \in \mathbb{S}^2$ is the unit vector

$$\mathring{\mathbf{d}} \cong \begin{pmatrix} C_2^0 - C_0^0 \\ C_1^1 - C_0^1 \\ C_1^2 - C_0^2 \end{pmatrix}, \tag{1}$$

where $\cong$ denotes equality up to positive scalar multiplication. Its moment shall be the unit vector $\mathring{\mathbf{m}} \in \mathbb{S}^2$

$$\mathring{\mathbf{m}} \cong \begin{pmatrix} C_2^0 \\ C_1^1 \\ C_1^2 \end{pmatrix} \times \begin{pmatrix} C_0^0 \\ C_0^1 \\ C_0^2 \end{pmatrix}, \tag{2}$$

which is the normal to the plane which contains both the baseline and the origin.

B. Rectification by Re-Projection

Our goal is to project both images to a virtual detector with an image u-axis pointing in the direction of the stereo baseline. Assuming that the iso-center is approximately in the coordinate origin, a good choice of virtual detector plane is

$$\mathbf{e} \cong \begin{pmatrix} \mathring{\mathbf{d}} \times \mathring{\mathbf{m}} \\ 0 \end{pmatrix} \in \mathbb{P}^3. \tag{3}$$

Since the u-axis must point in direction of the baseline, we establish a 2D coordinate frame for points in the plane $\mathbf{e}$ with 3D coordinate axis directions $\mathring{\mathbf{d}}$ and $\mathring{\mathbf{m}}$ according to

$$\mathbf{S} = \begin{pmatrix} \mathring{\mathbf{d}}^\top & 0 \\ \mathring{\mathbf{m}}^\top & 0 \\ \mathbf{0} & m \end{pmatrix} \in \mathbb{R}^{3\times 4}. \tag{4}$$

with arbitrary pixel size m in mm. Given an original image with projection matrix $\mathbf{P}$ and source position $\mathbf{c} \in \text{null}(\mathbf{P})$, let $\mathbf{T}_\mathbf{c}^\mathbf{e} \in \mathbb{R}^{4\times 4}$ denote the central projection through $\mathbf{c}$ to 3D points on the virtual detector plane $\mathbf{e}$ (compare Section II-C) and $\mathbf{S}$ defined its 2D coordinate system. Then, the homography

$$\mathbf{H} = \mathbf{S}\mathbf{T}_\mathbf{c}^\mathbf{e}\mathbf{P}^+ \in \mathbb{R}^{3\times 3}, \tag{5}$$

directly relates pixels from the original image with pixels in the virtual detector plane $\mathbf{e}$. This situation is visualized in Figure 1.

C. Central Projection onto a Plane

Central projection from a point $\mathbf{c} \in \mathbb{P}^3$ to a plane $\mathbf{e} \in \mathbb{P}^3$ can be written in a single matrix $\mathbf{T}_\mathbf{c}^\mathbf{e} \in \mathbb{R}^{4\times 4}$. It projects a point $\mathbf{x} \in \mathbb{P}^3$ to a point $\mathbf{T}_\mathbf{c}^\mathbf{e}\mathbf{x} \in \mathbb{P}^3$ by intersection of the plane $\mathbf{e}$ with the line $\mathbf{r}$ through the points $\mathbf{c}$ and $\mathbf{x}$. Using the Plücker matrix [2] of the line $\mathbf{c}\mathbf{x}^\top - \mathbf{x}\mathbf{c}^\top$ we express the intersection as

$$\mathbf{T}_\mathbf{c}^\mathbf{e}\mathbf{x} = \mathbf{c}\mathbf{x}^\top\mathbf{e} - \mathbf{x}\mathbf{c}^\top\mathbf{e}. \tag{6}$$

By factoring out $\mathbf{x}$ we obtain the projection

$$\mathbf{T}_\mathbf{c}^\mathbf{e} = \mathbf{I}_4\mathbf{c}^\top\mathbf{e} - \mathbf{c}\mathbf{e}^\top, \tag{7}$$

We can rectify two projections with the homographies

$$\begin{aligned} \mathbf{H}_0 &= \mathbf{S}\mathbf{T}_{\mathbf{c}_0}^\mathbf{e}\mathbf{P}_0^+ \\ \text{and } \mathbf{H}_1 &= \mathbf{S}\mathbf{T}_{\mathbf{c}_1}^\mathbf{e}\mathbf{P}_1^+. \end{aligned} \tag{8}$$

III. The Radon Transform of Perspectively Distorted Functions

A. Line Integrals in Perspectivley Transformed Images

This section computes an integral along a line $\mathbf{l}'$ over an image which has been projectively transformed by a homography $\mathbf{H}$. We will express the integration over a line $\mathbf{l} = \mathbf{H}^\top\mathbf{l}'$ (see in Eq. 12) in the original image, weighted by the Jacobian. Let $\mathbf{l}$ be the line with angle to the u-axis α and signed distance to the origin τ

$$\mathbf{l} \cong \begin{pmatrix} l_0 \\ l_1 \\ l_2 \end{pmatrix} = \begin{pmatrix} \sin(\alpha) \\ -\cos(\alpha) \\ -\tau \end{pmatrix}. \tag{9}$$

We append a zero to the 2D vectors of its normal $\mathbf{n} = (l_0, l_1, 0)^\top$ and direction

$$\mathbf{d} = \begin{pmatrix} d_0 \\ d_1 \\ 0 \end{pmatrix} = \begin{pmatrix} l_1 \\ -l_0 \\ 0 \end{pmatrix}, \tag{10}$$

with unit length $\|\mathbf{n}\| = \|\mathbf{d}\| = 1$. The closest point to the origin is given by the homogeneous coordinates

$$\mathbf{o} \cong \begin{pmatrix} o_0 \\ o_1 \\ 1 \end{pmatrix} = \begin{pmatrix} -l_2 l_0 \\ -l_2 l_1 \\ 1 \end{pmatrix}. \tag{11}$$

Lines transform covariantly, therefore, the transformed line is given by

$$\mathbf{H}^{-\top}\mathbf{l} \cong \mathbf{l}' = \begin{pmatrix} l_0' \\ l_1' \\ l_2' \end{pmatrix} = \begin{pmatrix} \sin(\alpha') \\ -\cos(\alpha') \\ -\tau' \end{pmatrix}, \tag{12}$$

with direction

$$\mathbf{d}' = \begin{pmatrix} l'_1 \\ -l'_0 \\ 0 \end{pmatrix}. \tag{13}$$

The Radon transform is the integral over a line in an image

$$\begin{aligned} \mathcal{R}f(\alpha,\, \tau) = \mathcal{R}f(\mathbf{l}) &= \int f(o_0 + d_0 \cdot t,\, o_1 + d_1 \cdot t)\, \mathrm{d}t \\ &\stackrel{\text{def}}{=} \int f_{\mathbf{l}}(t)\, \mathrm{d}t, \end{aligned} \tag{14}$$

where $f_{\mathbf{l}}(t)$ is the image defined over the 1D sub-space parametrized by the line-coordinate t. Since a projective transformation $\mathbf{H}$ on the image is collinearity preserving, a mapping $\varphi(t) :\, t \mapsto t'$ must exist which fulfills

$$\mathcal{R}\mathbf{H}f(\alpha', \tau') = \mathcal{R}\mathbf{H}f(\mathbf{l}') = \int f_{\mathbf{l}}\left(\varphi^{-1}(t')\right)\, \mathrm{d}t', \tag{15}$$

where $\mathbf{H}f$ denotes the transformed image and t' is the line coordinate along the transformed line $\mathbf{l}'$. Equation 15 shows that only information on the original line $f_{\mathbf{l}}$ is required for this computation of $\mathcal{R}\mathbf{H}f(\mathbf{l}')$. A change of variables with $t' = \varphi(t)$ yields

$$\mathcal{R}\mathbf{H}f(\mathbf{l}') = \int f_{\mathbf{l}}\,(t)\, \frac{\partial}{\partial t}\varphi(t)\, \mathrm{d}t. \tag{16}$$

B. Projection to Line Coordinates

The goal of this section is to find a closed form for $\varphi(t)$ in Equation 15, by considering only the line coordinate t on the line $\mathbf{l}$ and t' on the line $\mathbf{l}'$. Because the Jacobian of a rigid transformation is one, we can consider w.l.o.g. the case of $\mathbf{l}_u = (0, 1, 0)^\top$, which is related to the line $\mathbf{l}$ with the rigid transformation

$$\mathbf{H}_{\mathbf{l}u} = \begin{pmatrix} l_1 & -l_0 & 0 \\ l_0 & l_1 & l_2 \\ 0 & 0 & 1 \end{pmatrix} \text{ with } \begin{pmatrix} 0 \\ 1 \\ 0 \end{pmatrix} = \mathbf{H}_{\mathbf{l}u}^{-\top}\mathbf{l}. \tag{17}$$

Here, $\mathbf{H}_{\mathbf{l}u}$ takes image points $\mathbf{x} = (u,\, v,\, 1)^\top$ on the line $\mathbf{l}$ in the domain of the image $f(u, v)$ to line coordinates in the domain of $f_{\mathbf{l}}(t)$

$$\mathbf{x} = \mathbf{o} + \mathbf{d}t = \mathbf{H}_{\mathbf{l}u}^{-1} \begin{pmatrix} t \\ 0 \\ 1 \end{pmatrix} \text{ with } \mathbf{x}^\top\mathbf{l} = 0. \tag{18}$$

Analogously, we can transform line coordinates on $\mathbf{l}'$ with $\mathbf{H}_{\mathbf{l}'u}$ according to

$$\begin{pmatrix} t' \\ 0 \\ 1 \end{pmatrix} = \mathbf{H}_{\mathbf{l}'u}\mathbf{x}' \text{ iff. } \mathbf{x}'^\top\mathbf{l}' = 0. \tag{19}$$

However, if $\mathbf{H}$ is a rectifying homography according to Equation 8 and if $\mathbf{l}$ is an epipolar line, then $\mathbf{d}' = (1,\, 0,\, 0)^\top$ by definition and $\mathbf{H}_{\mathbf{l}'u}$ is only a translation.

C. Line-Induced Perspectivity

Using Equations 18 and 19 we have

$$\begin{aligned} & \mathbf{x}' \cong \mathbf{H}\mathbf{x} \\ \iff \quad & \mathbf{H}_{\mathbf{l}'u}^{-1} \begin{pmatrix} t' \\ 0 \\ 1 \end{pmatrix} \cong \mathbf{H}\mathbf{H}_{\mathbf{l}u}^{-1} \begin{pmatrix} t \\ 0 \\ 1 \end{pmatrix} \\ \iff \quad & \begin{pmatrix} t' \\ 0 \\ 1 \end{pmatrix} \cong \underbrace{\mathbf{H}_{\mathbf{l}'u}\mathbf{H}\mathbf{H}_{\mathbf{l}u}^{-1}}_{\mathbf{J}} \begin{pmatrix} t \\ 0 \\ 1 \end{pmatrix}. \end{aligned} \tag{20}$$

Since both sides of the equation contain a zero-element, only the four corner elements of the the matrix $\mathbf{J}$ are relevant. Note that $\mathbf{H}_{\mathbf{l}u}^{-1}$ and $\mathbf{H}_{\mathbf{l}'u}$ can be elegantly written by column, respectively, row vectors

$$\mathbf{H}_{\mathbf{l}u}^{-1} = \begin{pmatrix} | & | & | \\ \mathbf{d} & \mathbf{n} & \mathbf{o} \\ | & | & | \end{pmatrix}, \tag{21}$$

and

$$\mathbf{H}_{\mathbf{l}'u} = \begin{pmatrix} - & \mathbf{d}'^\top & - \\ - & \mathbf{l}'^\top & - \\ 0 & 0 & 1 \end{pmatrix}. \tag{22}$$

The entries of $\mathbf{l}$ can be computed via Equation 20, while we are only interested in the case where $\mathbf{H}$ is a rectifying homography and $\mathbf{l}$ is an epipolar line, we have more compactly, $\mathbf{d}' = (1,\, 0,\, 0)^\top$ and

$$J_{00} = \mathbf{d}'^\top\mathbf{H}\mathbf{d} \qquad = h_{00}l_1 - h_{10}l_0, \tag{23}$$

$$J_{02} = \mathbf{d}'^\top\mathbf{H}\mathbf{o} \qquad = h_{02} \quad - h_{00}l_0l_2, \tag{24}$$

$$J_{20} = (0,\, 0,\, 1) \cdot \mathbf{H}\mathbf{d} \quad = h_{20}l_1 - h_{21}l_0, \tag{25}$$

$$J_{22} = (0,\, 0,\, 1) \cdot \mathbf{H}\mathbf{o} \quad = h_{22} \quad - h_{20}l_0l_2 - h_{21}l_1l_2. \tag{26}$$

Assuming that the horizon is not contained in the support of f, de-homogenization of the mapping from $\mathbb{P}^1$ coordinates on the line $\mathbf{l}$ to $\mathbb{P}^1$ coordinates on the line $\mathbf{l}'$ is written

$$t' = \varphi(t) = \frac{J_{00} \cdot t + J_{02}}{J_{20} \cdot t + J_{22}}, \tag{27}$$

and

$$\frac{\partial}{\partial t}\varphi(t) = \frac{J_{00}J_{22} - J_{02}J_{10}}{J_{20}^2t^2 + 2 \cdot J_{20}J_{22} \cdot t + J_{22}^2}. \tag{28}$$

The Radon transform for a line $\mathbf{l}'$ can thus be computed using regular ray-casting in f by weighting each sample $\mathbf{x} = \mathbf{o} + t \cdot \mathbf{d}$ with $\frac{\partial}{\partial t}\varphi(t)$. For some regular sampling distance Δt in the original image (typically about 0.66 px), we have

$$\mathcal{R}\mathbf{H}f(\mathbf{l}') \approx \Delta t \sum_i \left.\frac{f(\mathbf{o} + t \cdot \mathbf{d}) \cdot (J_{00}J_{22} - J_{02}J_{20})}{J_{20}^2t^2 + 2 \cdot J_{20}J_{22} \cdot t + J_{22}^2}\right|_{t = i \cdot \Delta t}, \tag{29}$$

with the original line

$$\mathbf{l} \cong \mathbf{H}^\top\mathbf{l}' = \mathbf{H}^\top \begin{pmatrix} \sin(\alpha') \\ -\cos(\alpha') \\ -\tau' \end{pmatrix}. \tag{30}$$

IV. Discussion

We have presented a general and fast algorithm for evaluation of fan-beam DCCs on a virtual detector plane based on Lesaint et al. [4], which also handles non-circular trajectories. We have shown that reprojection to a common virtual detector is an instance of stereo rectification. However, rectifying each pair of projections, requires $n \cdot (n-1)$ rectified 2D images. In Figure 2 we show that rectification increasingly distorts the images, as the angle between the primary rays increases. For proper sampling rectified images would have to be considerably larger than the original projections, rendering the original algorithm impractical. We show how to compute line integrals over projectively transformed images on the fly, i.e. directly from the original projection image data, which is drastically faster and requires no additional memory. This

Algorithm 1 Radon transform of a projectively distorted image $\mathbf{H}f$ for a line $\mathbf{l}' = \mathbf{H}^{-\top}\mathbf{l}$ from original image f.

- **input** – Line $\mathbf{l}' = (\sin(\alpha'), -\cos(\alpha'), -\tau)^\top$
  – Homography $\mathbf{H} \in \mathbb{R}^{3\times3}$ (as in Equation 8).

1) Compute $\mathbf{l}$ according to Equation 30, its closest point $\mathbf{o}$ (Equation 11), and direction $\mathbf{d}$ (Equation 10).
2) Normalize $\|\mathbf{n}\| = \|\mathbf{d}\| = 1$ and dehomogenize $o_2 = 1$.
3) Compute J_{00} to J_{22} according to Equations 23-26.
4) Compute values t_{min} and t_{max}, such that $\mathbf{x}_{min} = \mathbf{o} + t_{min} \cdot \mathbf{d}$ and $\mathbf{x}_{max} = \mathbf{o} + t_{max} \cdot \mathbf{d}$ are the intersections of the line with the image border with $t_{min} < t_{max}$.
5) Initialize summation variable s.
6) **for** ($t = t_{min}$; $t \leq t_{max}$; $t \leftarrow t + \Delta t$)
   a) Compute pixel location $\mathbf{x} \leftarrow \mathbf{o} + t \cdot \mathbf{d}$
   b) Compute $j \leftarrow \frac{\partial}{\partial t}\varphi(t)$ according to Equation 28.
   c) Compute distance w of 3D location of $\mathbf{x}$ (on the virtual detector) to the source position.[4], [5]
   d) Increment $s \leftarrow s + f(\mathbf{x}) \cdot j \cdot w \cdot \Delta t$.
7) **return** Variable s, which is the Radon transform of projectively distorted image $\mathbf{H}f$ for a line $\mathbf{l}'$.

paper gives a general implementation for this situation. For validation, we present in Figure 4, top, the redundant signals extracted from two X-ray shots of a pumpkin, along with the warped images in Figure 3. The fan-beam consistency condition can be computed explicitly as a sum over these rectified images weighted by the distance of each point to the stereo baseline. Integration in the original images, while taking into account the Jacobian according to Algorithm 1 is identical. The method breaks down for large primary angle difference, once the epipoles lie within the images, compare Figure 2, right. To demonstrate the fundamentally different nature of this consistency condition by comparison with epipolar consistency for the same epipolar planes in Figure 4, bottom. Since EC is based on a derivative orthogonal to the lines, we observe a roughly zero-mean curve and more detail for smaller structures. Generally speaking, rectification-based methods will be slower than their deriative-based counterparts for motion- and calibration-correction, because the Radon intermediate functions cannot be pre-computed. Future work will investigate, if avoidance of the derivative has potential benefits in applications, where absolute intensity values need to be estimated, such as beam-hardening, scatter correction or metal-artifact correction. Future work will investigate how the presented epipolar DCCs are affected by truncation and we will compare other DCCs.

Acknowledgments: This work is supported by the German Research Foundation; DFG MA 4898/3-1 "Consistency Conditions for Artifact Reduction in Cone-beam CT" and partially supported by the Agence Nationale de la Recherche (France), Labex CAMI, number ANR-11-LABX-0004-01 and project "DROITE", number ANR-12-BS01-0018. We thank NVIDIA Corporation for the donation of a Titan Xp GPU.

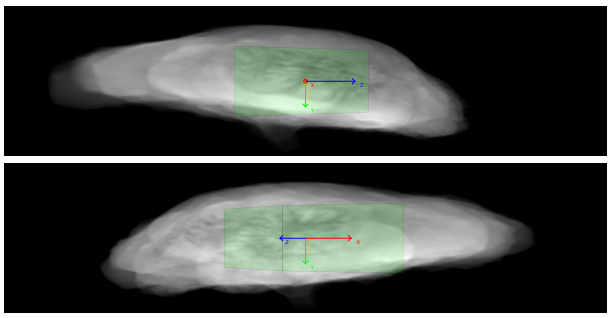

Figure 3. Rectified projection images of a pumpkin phantom in case of a primary angle difference of 120°. The green cube is intended to visualize the distortion introduced by rectification.

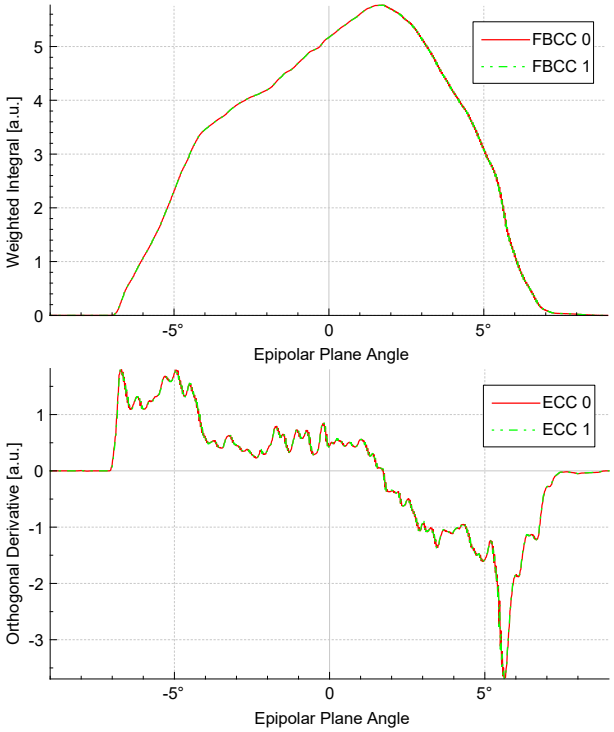

Figure 4. Top: Fan-beam consistency condition (FBCC) [5] as implemented in the original images. The computation of the rectified images in Figure 3 is avoided, but the curves are identical to a weighted summation over the intensity in these images. Bottom: Comparison to epipolar consistency conditions (ECC) for the same images (i.e. orthogonal derivative instead of rectification and weighting) is shown for corresponding epipolar plane angles.

References

[1] A. Aichert, K. Breininger, T. Köhler, and A. Maier. Efficient epipolar consistency. In *4th International Conference on Image Formation in X-Ray Computed Tomography*, pages 383–386, 2016.

[2] R. I. Hartley and A. Zisserman. *Multiple View Geometry in Computer Vision*. Cambridge University Press, ISBN: 0521623049, 2000.

[3] J. Lesaint, R. Clackdoyle, S. Rit, and L. Desbat. Two cone-beam consistency conditions for a circular trajectory. In *Proc. 4th Int. Conf. Image Formation X-Ray Comput. Tomography*, pages 431–434, 2016.

[4] J. Lesaint, S. Rit, R. Clackdoyle, and L. Desbat. Calibration for circular cone-beam ct based on consistency conditions. *IEEE Transactions on Radiation and Plasma Medical Sciences*, 1(6):517–526, 2017.

[5] M. S. Levine, E. Y. Sidky, and X. Pan. Consistency conditions for cone-beam ct data acquired with a straight-line source trajectory. *Tsinghua Sci Technol.*, 15(1):56–61, Feb 2010.